





RESEARCH ARTICLE

Widespread tissue hypoxia dysregulates cell and metabolic pathways in SMA

Elena Hernandez-Gerez^{1,2}, Sergio Dall'Angelo^{1,3} , Jon M. Collinson¹ , Ian N. Fleming^{1,a}  & Simon H. Parson^{1,2,a} 

¹Institute of Medical Sciences, School of Medicine, Medical Sciences and Nutrition, University of Aberdeen, Foresterhill, Aberdeen, AB25 2ZD, UK

²Euan Macdonald Centre for Motor Neurone Disease Research, University of Edinburgh, Chancellor's Building, Edinburgh, EH16 4SB, UK

³John Mallard Scottish PET Centre, University of Aberdeen, Foresterhill, AB25 2ZD, UK

Correspondence

Simon H. Parson, Anatomy, Suttie Centre, School of Medicine, Medical Sciences and Nutrition, University of Aberdeen, Foresterhill, Aberdeen AB25 2ZD, UK. Tel: 01224 274328; E-mail: simon.parson@abdn.ac.uk

Funding Information

SMA Europe (SMA UK and Prinses Beatrix Spierfonds).

Received: 16 June 2020; Accepted: 1 July 2020

Annals of Clinical and Translational Neurology 2020; 7(9): 1580–1593

doi: 10.1002/acn3.51134

^aThese authors contributed equally

Abstract

Objective: The purpose of the study was to determine the extent and role of systemic hypoxia in the pathogenesis of spinal muscular atrophy (SMA). **Methods:** Hypoxia was assayed *in vivo* in early-symptomatic (postnatal day 5) SMA-model mice by pimonidazole and [¹⁸F]-Fluoroazomycin arabinoside injections, which accumulate in hypoxic cells, followed by immunohistochemistry and tracer biodistribution evaluation. Glucose uptake in hypoxic cells was assayed by [¹⁸F]-Fluorodeoxyglucose labeling. *In vitro* knockdown of Survival Motor Neuron (SMN) was performed on motor neurons and lactate metabolism measured biochemically, whereas cell cycle progression and cell death were assayed by flow cytometry. **Results:** All assays found significant levels of hypoxia in multiple organ systems in early symptomatic SMA mouse pups, except aerated tissues such as skin and lungs. This was accompanied by significantly increased glucose uptake in many affected organs, consistent with a metabolic hypoxia response. SMN protein levels were shown to vary widely between motor neuron precursors *in vitro*, and those with lower levels were most susceptible to cell death. In addition, SMA-model motor neurons were particularly sensitive to hypoxia, with reduced ability to transport lactate out of the cell in hypoxic culture, and a failure in normal cell cycle progression. **Interpretation:** Not only is there widespread tissue hypoxia and multi-organ cellular hypoxic response in SMA model mice, but SMA-model motor neurons are especially susceptible to that hypoxia. The data support the hypothesis that vascular defects leading to hypoxia are a significant contributor to disease progression in SMA, and offer a route for combinatorial, non-SMN related therapy.

Introduction

Spinal muscular atrophy (SMA) is a predominately early onset childhood neurodegenerative disease caused by homozygous mutation of the Survival Motor Neuron 1 (*SMN1*) gene.¹ The *SMN1* gene is the main producer of the ubiquitous Survival Motor Neuron (SMN) protein, with a wide range of functions mainly related to RNA metabolism.² Its complete absence is lethal at the embryonic stage,³ but in contrast to most mammals that have only a single *SMN* gene, humans also have a Survival Motor Neuron 2 (*SMN2*) paralogue. This is identical to *SMN1* save for a single base-pair splice site mutation

which predisposes to inappropriate removal of exon 7 from the mRNA, yielding a nonfunctional truncated protein. *SMN2* only produces a small amount of functional, correctly spliced, SMN protein. This is sufficient for survival to birth but not to allow for normal postnatal health.¹

It is becoming increasingly evident that this cell-ubiquitous reduction of SMN results not only in a neurodegenerative but also a vascular disease. Necrosis at the tip of toes and fingers has been observed in patients, as well as thrombotic occlusions of small vessels,⁴ together with significant reductions in vascular density in the mouse models of severe SMA,⁵ these symptoms suggest defects in

blood supply. In fact SMA mouse spinal cord is hypoxic,⁵ suggesting that other tissues may also be affected.

All tissues can be damaged by hypoxia, but motor neurons are particularly sensitive.⁶ As neurodegeneration is the major pathological event in SMA, hypoxia may be a significant co-morbidity. Vascular defects have been found in other neurodegenerative diseases such as amyotrophic lateral sclerosis and multiple sclerosis, suggesting that hypoxia could be a previously overlooked factor in neuronal degeneration in motor neuron diseases.⁷ In addition, SMN splicing is negatively affected by hypoxia, further reducing the amount of functional protein,⁸ and likely exaggerating disease pathology.

Historically, non-neuronal pathology has been of less interest, as the severe motor neuron pathology negated the need to consider additional therapies. However, now that treatments have become available, including Nusinersen (Spinraza) and Onasemnogene abeparvovec (Zolgensma),⁹ survival is increasing, but so is the likelihood of significant non-neuronal co-morbidities. The first child treated with Nusinersen (Spinraza) is now 7 years old, but this is still only a short way into what is hoped will be a normal lifespan, and it will be important to continue to monitor these children closely. The factors downstream of SMN reduction leading to SMA pathology remain largely unknown, but if we understand functional pathologies we can target them with non-SMN related combinatorial therapies. Tissue hypoxia could be targeted with oxygenation therapies,¹⁰ whereas damage due to cellular hypoxia can be targeted pharmacologically.¹¹

There is therefore an urgent need to better understand the extent to which established cardiovascular pathologies result in functional tissue and cellular hypoxia, and what the responses of SMN-knockdown cells to this hypoxia are.

Here we systematically map tissue hypoxia in a severe mouse model of SMA, and go on to determine the vulnerability of low SMN cells to hypoxia and the downstream metabolic consequences of hypoxia in SMA. We show that hypoxia is widespread, that low-SMN cells are particularly sensitive to it, triggering metabolic dysregulation, cell-cycle arrest, and cell death.

Materials and Methods

Animals

The model used for this work was the “Taiwanese” SMA¹² mouse model. Viable, fertile parental lines [*Smn*^{-/-}; *SMN2*^{tg/tg}] and *Smn*^{+/-} (Jackson laboratory stock number 5058) were maintained at the Medical Research Facility at University of Aberdeen on woodchip with sawdust, paper bedding, environmental enrichment, and food and water

ad libitum. The lines were crossed to yield litters with [*Smn*^{-/-}; *SMN2*^{tg/0}] pups that model severe SMA (henceforth “SMA mice”) and littermate, heterozygous control [*Smn*^{+/-}; *SMN2*^{tg/0}] healthy pups. The day of birth was designated as P0.

All animal experiments were approved by University of Aberdeen ethics committees and carried out under appropriate personal and project licenses granted by United Kingdom Home Office under the Animals (Scientific Procedures) Act 1986.

[¹⁸F]-FAZA and [¹⁸F]-FDG experiments in mice

[¹⁸F]-Fluorodeoxyglucose ([¹⁸F]-FDG) and [¹⁸F]-Fluorazomycin arabinoside [¹⁸F]-FAZA were synthesized according to standard protocols developed at the John Mallard PET Centre.

[¹⁸F]-FAZA (0.1–0.5 MBq/g) or [¹⁸F]-FDG (0.2 MBq/g) was administered by intravenous (IV) injection to P5 mice after anesthesia with isoflurane. Mice were left for 90 minutes prior to culling by cervical dislocation and decapitation, in accordance with UK guidance and rules for the use of animals in research. Each tissue of interest was then collected by dissection and weighed. Radioactivity taken up by each tissue was measured using a well counter with a Nuclear Instruments (Oakland UK) interface until at least 1000 counts were accumulated. Radioactivity uptake was analyzed as counts per minute per gram of tissue per MBq of radiotracer injected. The recorded data were analyzed by Student’s *t*-test using Graphpad Prism®.

Pimonidazole experiments in mice

Pimonidazole (60 µg/g body mass) was administered by intravenous (IV) injection to P5 mice after anesthesia with isoflurane. Mice were culled by cervical dislocation and decapitation 24 hours after injections and tissue collected, in accordance with UK the guidance and rules for the use of animals in research.

Tissue collection

Tissue for immunostaining was immediately fixed in 4% paraformaldehyde (PFA) w/v in phosphate-buffered saline (PBS) after collection. Liver, heart, spleen, brain, and kidney were fixed for 4 hours. Spinal cord was fixed for 24 hours. Tissue was washed three times in PBS then submerged in 30% sucrose for cryoprotection and then frozen in OCT.

Tissue for western blotting was immediately frozen in dry ice and stored at –80°C.

Immunocytochemistry

Ten micrometer cryosections were stained with FITC-conjugated antipimonidazole mouse IgG1 monoclonal antibody (Hypoxyprobe, HP Mab1) at 1:50 concentration. They were then stained with HRP-bound anti-FITC antibody (Hypoxyprobe, anti-FITC-HRP) and incubated with DAB staining solution (Vector, SK-4100). Coverslips were mounted with CV Mount (Leica) at the Histology Core Facility at the University of Aberdeen before imaging.

Quantitative fluorescent western blot analysis

Tissue was digested in RIPA buffer with 2.5% Protease inhibitor cocktail (Sigma-Aldrich, P8340). Western blot analysis was performed as described¹³ Protein levels were assessed with Licor Biosciences REVERT Total Protein Stain Kit (Licor Biosciences, 926-11010). HIF-1 was labeled with 1:500 Anti-HIF-1 α antibody (Abcam, ab2185), HIF-2 with Anti-HIF-2 α antibody (Abcam, ab109616). Imaging was done with Odyssey[®] CLx LICOR imaging system. The density of each protein band was measured using Image Studio Lite and the resulting data were compared with Student's *t*-test considering $P < 0.05$ as significant.

Cell culture

NSC-34 neurons were cultured under sterile conditions in DMEM media containing 1% L-glutamine, 1% Penicillin/Streptomycin, and 10% FBS in T75 flasks at 37°C in a humidified atmosphere containing 5% CO₂.

Transfection

NSC-34 neurons were transfected with s74016 Silencer select siRNA (Thermo Fisher) at a 100 nM concentration with jetPRIME[®] (Source Bioscience) following the manufacturer's instructions. After transfection cells were routinely incubated for 72 hours before starting any further experiments to maximize SMN protein downregulation.

Simulation of hypoxic insult

Cells were incubated in a hypoxic in vitro cabinet (Coylabs) regulated by an oxygen controller (Coylabs) as outlined previously,¹³ with oxygen levels set at 1% O₂.

Flow cytometry for SMN levels

Cells were collected by trypsinization and combined with medium containing any floating (dead) cells. For SMN

and cell death experiments, cells were incubated on ice for 30 minutes with Fixable Viability Stain 450 (BD Horizon, 562247) at 1 μ L/mL concentration after collection, then fixed in 4% PFA in PBS for 15 minutes at 4°C and then permeabilized with 90% methanol for 30 minutes at 4°C. Samples were incubated for 1h at 4°C with Anti-SMN Antibody, clone 2B1 (05-1532, Merck). Samples were then incubated for 30 minutes on ice with the secondary antibody Goat anti-Mouse IgG1 Secondary Antibody, Alexa Fluor 488 (A21121, ThermoFisher). In each experiment data were taken from two independent experiments, so the fluorescent signal was normalized to the mean of the normoxic control samples, to avoid laser emission variances across experiments, which affect fluorescence signal intensity. Cell cycle analysis was performed as described.¹⁴ All work was carried out in the Iain Fraser Cytometry Centre at the University of Aberdeen, using the BD LSR II flow cytometer. Data were collected with DIVA software. Data were analyzed with FlowJo software (FlowJo, LLC).

L-lactate assay

Cells were grown in 6-well plates. Hypoxic samples were grown in hypoxia for 24 hours before collecting cell medium (2ml), for extracellular lactate, and cell lysates (200ml), for intracellular lactate. L-lactate was detected with L-Lactate assay kit (Abcam, ab65330).

Results

Hypoxia is widespread in neuronal and non-neuronal tissues in pre/early-symptomatic SMA mice

SMA mouse spinal cord has been shown to be hypovascular and hypoxic.⁵ However, several other tissues and organs of severe SMA mice also have lower capillary density and capillary developmental defects compared with their healthy counterparts,^{5,15,16} but it is not known if they are also hypoxic. We therefore carried out a systematic assessment of hypoxia in early symptomatic postnatal day 5 (P5), "Taiwanese" model SMA mice, using *Smn*^{+/-} heterozygotes as controls. Mice were injected with pimonidazole, a hypoxia marker, detected postmortem by immunostaining with an HRP-bound antibody. We first confirmed hypoxia in SMA spinal cords by the presence of the dark, DAB, reaction product (data not shown). We found evidence of extensive hypoxia in other tissues; SMA brain showed the most pronounced evidence of hypoxia, with significant staining in the cortex (Figure 1A,B). Limb muscle showed small and scarce hypoxic areas (Figure 1C, D). In addition, kidney and spleen both showed large,

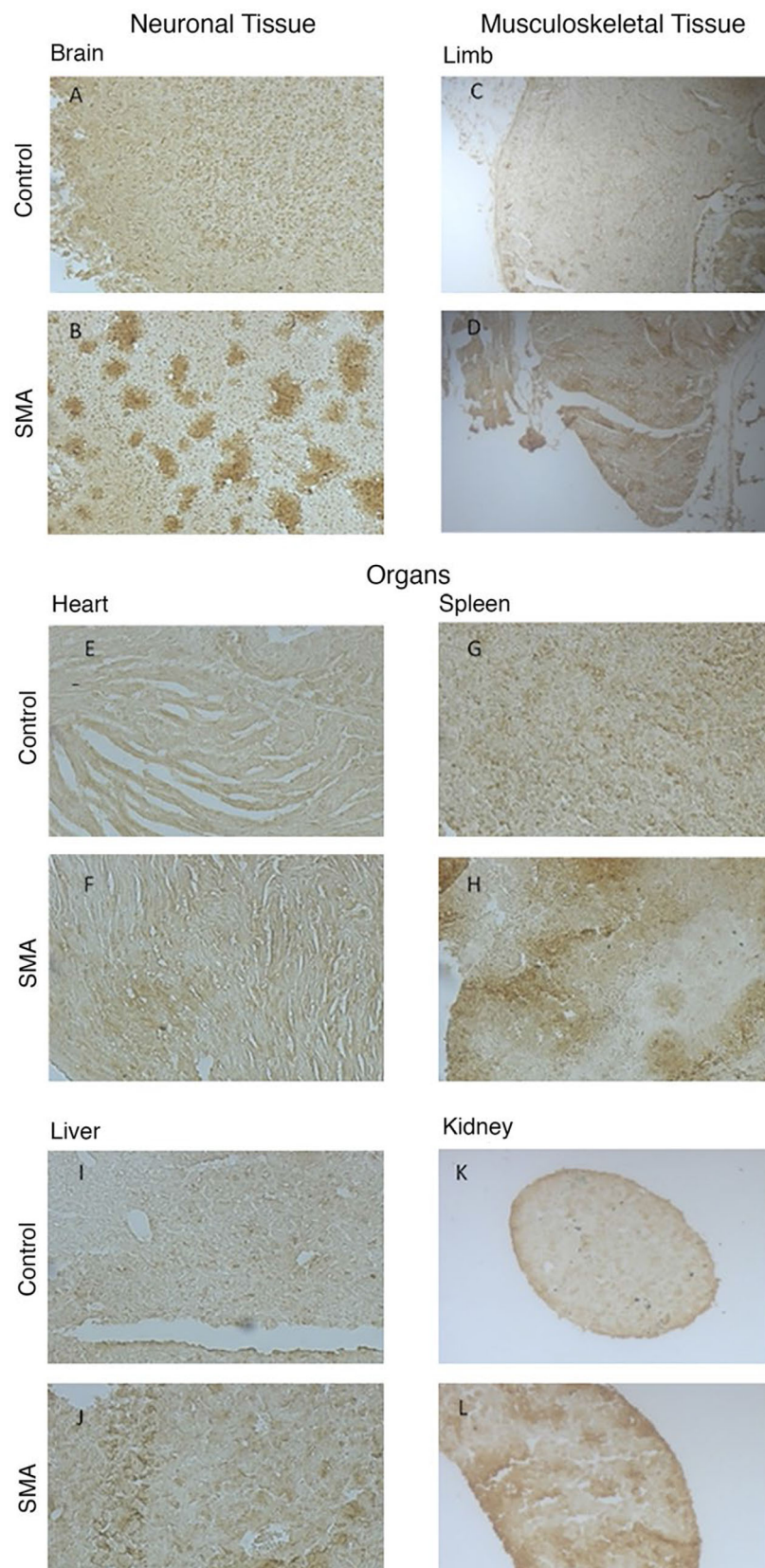


Figure 1. Pimonidazole labeling shows widespread hypoxia in SMA. To test for hypoxia in SMA tissue, presymptomatic 5-day-old “Taiwanese” model SMA mice were injected with Pimonidazole, a hypoxia marker ($n = 3$ mice). Pimonidazole labeling was visualized postmortem with an HRP-bound antibody for DAB staining. The staining shows widespread large hypoxic areas in brain (A,B), spleen (G,H), and kidney (K,L). Brain hypoxic areas are discrete and very defined, whereas kidney and spleen show larger more diffuse areas, sometimes interconnecting. Liver (I,J) show also smaller scarcer hypoxic areas, similarly to forelimb (C,D). The hypoxic areas seem to be more isolated in liver than in forelimb, where they appear to be close together. Hindlimb show wide hypoxic areas that tend to be diffuse at the margins. Control and SMA heart (E,F) do not show any noticeable differences. Scale bar = 100 μm .

diffuse areas of hypoxia staining (Figure 1G,H,K,L), whereas the liver showed small, isolated hypoxic areas (Figure 1I,J). In addition, by contrast, SMA heart showed no evidence of hypoxia (Figure 1E,F).

To confirm and extend these results, we next quantified hypoxia in the P5 SMA mice, by injecting a radiotracer ^{18}F -Fluoroazomycin arabinoside (^{18}F -FAZA) that is specifically retained in hypoxic cells.¹⁷ Postmortem measurement of radiotracer in isolated organs and tissues, indicative of hypoxia showed significantly higher levels in SMA tissues compared to controls: ~22% in brain, ~30% in spinal cord, ~31% in eye, ~46% in hindlimb muscle, ~19% in forelimb muscle, ~48% in tail, ~19% in kidney, ~51% in spleen, ~51% in liver, and ~28% in heart. Importantly, tissues such as skin and lungs which can take up atmospheric oxygen, showed no significant differences (Figure 2A). Taken together these observations show for the first time that the cardiovascular defects in heart, blood vessels, and circulating cells¹⁶ in SMA, are correlated with widespread and significant functional tissue hypoxia in neuronal and non-neuronal tissues. Importantly, this precedes any overt symptoms, and likely contributes to or exacerbates motor neuron loss.

Glucose uptake is dysregulated in SMA mice

Pimonidazole and ^{18}F -FAZA demonstrated widespread, quantifiable hypoxia in SMA, we therefore next investigated what functional consequences were associated with this tissue hypoxia. One of the most common metabolic changes in hypoxic tissue is the upregulation of glucose uptake. To look for changes in glucose uptake, P5 SMA mice were injected with ^{18}F -Fluorodeoxyglucose (^{18}F -FDG), a radioactive glucose analogue that is taken up and retained in cells. Mice were killed 90 minutes after exposure to ^{18}F -FDG, tissues and organs were harvested and ^{18}F -FDG signal analyzed. Any changes in glucose metabolism will result in changes in ^{18}F -FDG uptake and retention in cells. Central nervous system structures in SMA mice showed increased glucose uptake: ~58% in spinal cord, ~94% in brain, and ~67% in eye. The only non-neuronal tissues that showed a significant change in ^{18}F -FDG uptake were kidneys with a ~101% increase and heart

which showed a ~67% decrease in glucose uptake in SMA mice compared to controls. Spleen, liver, hindlimb, forelimb, and tail showed no significant differences between SMA and control littermates (Figure 3A). These data suggest that glucose uptake is dysregulated in multiple SMA organs and tissues, indicative of downstream metabolic changes in response to tissue hypoxia. Not all tissues labeled with ^{18}F -FAZA were labeled with ^{18}F -FDG, which confirms that any study on hypoxia in SMA needs to be done with specific radiotracers for hypoxia.

SMA neurons accumulate lactate in response to hypoxia

Normally functioning cells will generate intracellular lactate when exposed to hypoxia, which is then rapidly transported out of the cell, resulting in an increase in extracellular lactate. We therefore next assayed extra and intracellular lactate in NSC-34 control and siRNA knockdown (SMA model) neurons. In normoxia, as expected levels of extracellular lactate were similar in control (scrambled siRNA) and SMN knockdown neurons (Figure 4A). Furthermore, a normal, significant increase ($P < 0.05$) in extracellular lactate (nmol/ μL , mean \pm SEM) was seen when control neurons were exposed to hypoxia (normoxia: 1.55 ± 0.05 , hypoxia: 2.54 ± 0.27) but importantly, there was no significant rise in extracellular lactate when SMA neurons were exposed to hypoxia. This suggested that either lactate was not being produced in SMA neurons, or it was not being transported out of the cells. We therefore next assayed intracellular lactate. Intracellular lactate levels (pmol/ μL , mean \pm SEM) were unchanged between control neurons in normoxia and hypoxia, showing efficient transport out of the cells, but ~30–60% higher in SMA neurons in hypoxia (129.2 ± 11.87) compared with either control neurons in hypoxia (46.11 ± 4.81 ; $P < 0.01$) or SMA neurons in normoxia (47.99 ± 1.07 ; $P < 0.01$). This suggests an inability of SMA neurons to efficiently transport lactate out of the cell, and a dysregulated response to hypoxia in SMA.

These data suggest that in response to hypoxia, SMA neurons show a very specific dysregulation of intracellular lactate levels, suggesting an inability to correctly handle

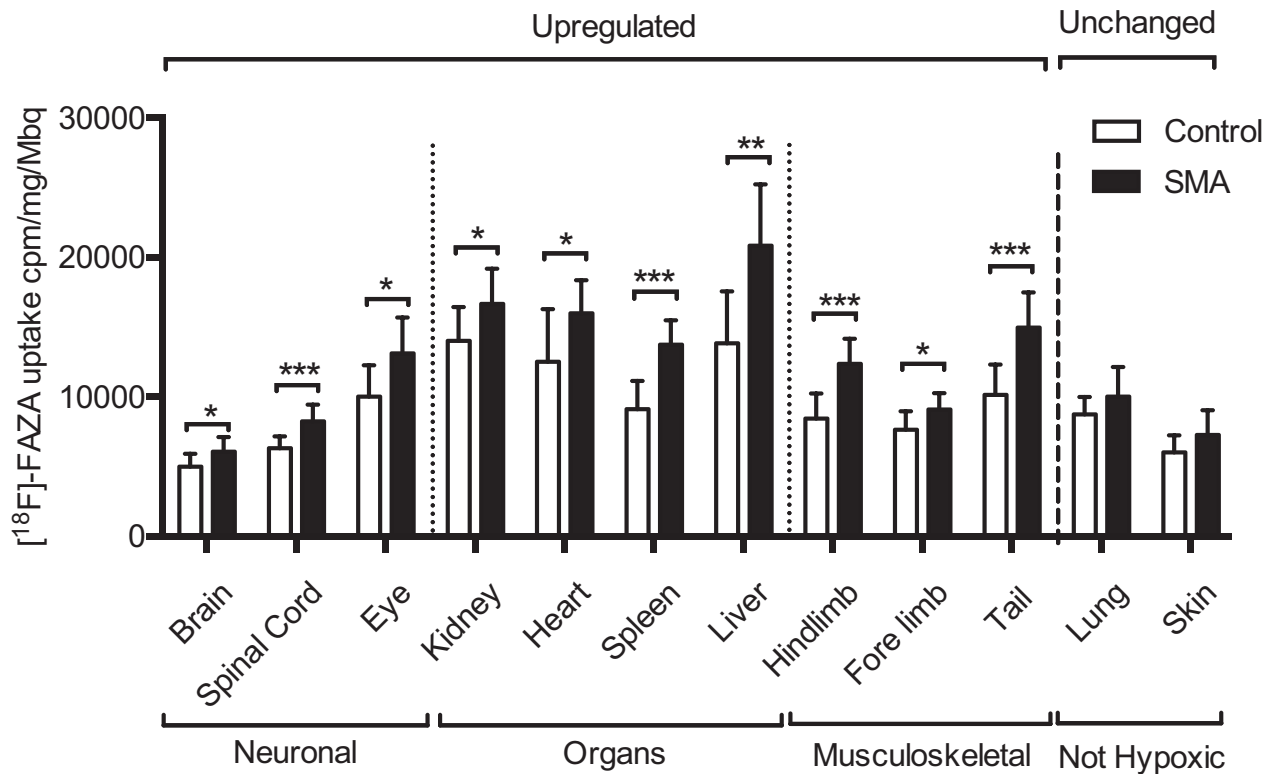


Figure 2. $[^{18}\text{F}]$ -FAZA uptake is higher in multiple tissues in SMA model mice. Presymptomatic 5-day-old Taiwanese mice were injected with the hypoxia-specific radiotracer $[^{18}\text{F}]$ -FAZA. Radioactivity was measured postmortem in counts per minute (cpm) with a well counter, and analyzed later as cpm per mg of tissue per MBq of tracer as a function of radioactivity injected ($n = 14$ control mice, 7 SMA mice). Heart, brain, eyes, spinal cord and kidneys, spleen, liver, hindlimb, forelimb, and tail in SMA pups showed upregulation of $[^{18}\text{F}]$ -FAZA uptake compared to their healthy counterparts, suggesting widespread hypoxia in SMA mouse model. $[^{18}\text{F}]$ -FAZA uptake remains similar in lungs and skin. In brains, mean $[^{18}\text{F}]$ -FAZA uptake was significantly increased in SMA mice by ~22% compared to control tissues (cpm/mg/MBq mean \pm SEM ($n = 3$): control = $4.98 \times 10^3 \pm 250$ ($n = 3$); SMA = $6.07 \times 10^3 \pm 396$ ($n = 3$); $P < 0.05$ *). In spinal cord, it was increased by ~30% (control = $6.32 \times 10^3 \pm 225$, SMA = $8.23 \times 10^3 \pm 453$; $P < 0.001$ ***), and by ~31% in eye (control = $1 \times 10^4 \pm 601$, SMA = $1.31 \times 10^4 \pm 977$; $P < 0.05$ *). In addition, musculoskeletal tissues: increased by ~46% in hindlimb (control = $8.44 \times 10^3 \pm 483$, SMA = $1.24 \times 10^4 \pm 686$; $P < 0.001$ ***), by ~19% in forelimb (control = $7.63 \times 10^3 \pm 356$, SMA = $9.10 \times 10^3 \pm 443$; $P < 0.05$ *) and by ~48% in tail (control = $1.01 \times 10^4 \pm 582$, SMA = $1.50 \times 10^4 \pm 957$; $P < 0.001$ ***). Finally, non-neuromuscular SMA tissues: $[^{18}\text{F}]$ -FAZA retention increased by ~19% in kidney (control = $1.40 \times 10^4 \pm 649$, SMA = $1.67 \times 10^4 \pm 953$; $P < 0.05$ *), by ~51% in spleen (control = $9.10 \times 10^3 \pm 544$, SMA = $1.37 \times 10^4 \pm 660$; $P < 0.001$ ***), by ~51% in liver (control = $1.38 \times 10^4 \pm 997$, SMA = $2.08 \times 10^4 \pm 1.7 \times 10^3$; $P < 0.01$ **), and by ~28% in heart (control = $1.25 \times 10^4 \pm 10^3$, SMA = $1.60 \times 10^4 \pm 894$; $P < 0.05$ *).

downstream metabolic changes occurring in response to hypoxia.

SMN protein levels in single neurons determines survival in hypoxia

Our data suggest that not only are SMA tissues hypoxic in vivo, but they are also particularly metabolically sensitive to hypoxia. Disease severity in SMA is known to correlate with total SMN protein levels,³ and these levels are known to vary from organ to organ,¹⁸ but very little is known about how SMN levels in individual cells determines key cellular outcomes, or indeed to what extent levels vary. We therefore next set out to determine the relationship between neuronal SMN levels and vulnerability. We

developed a flow cytometry protocol to measure and then plot the distribution of protein levels in single neurons. We initially quantified the levels of SMN protein in control and siRNA knockdown (SMA model) NSC-34 neurons. It was immediately apparent that both control and SMA neurons showed significant intrapopulation variability in SMN levels (Figure 5A). SMN protein levels were negatively skewed and varied over threefold from lowest to highest levels of expression in both SMA and control neurons. Single neuron SMN protein levels overlapped considerably, but peak, modal levels were lower in SMA neurons.

These data suggest that neurons with very low SMN levels are present in normal, control, presumed healthy populations of neurons, and conversely that neurons with

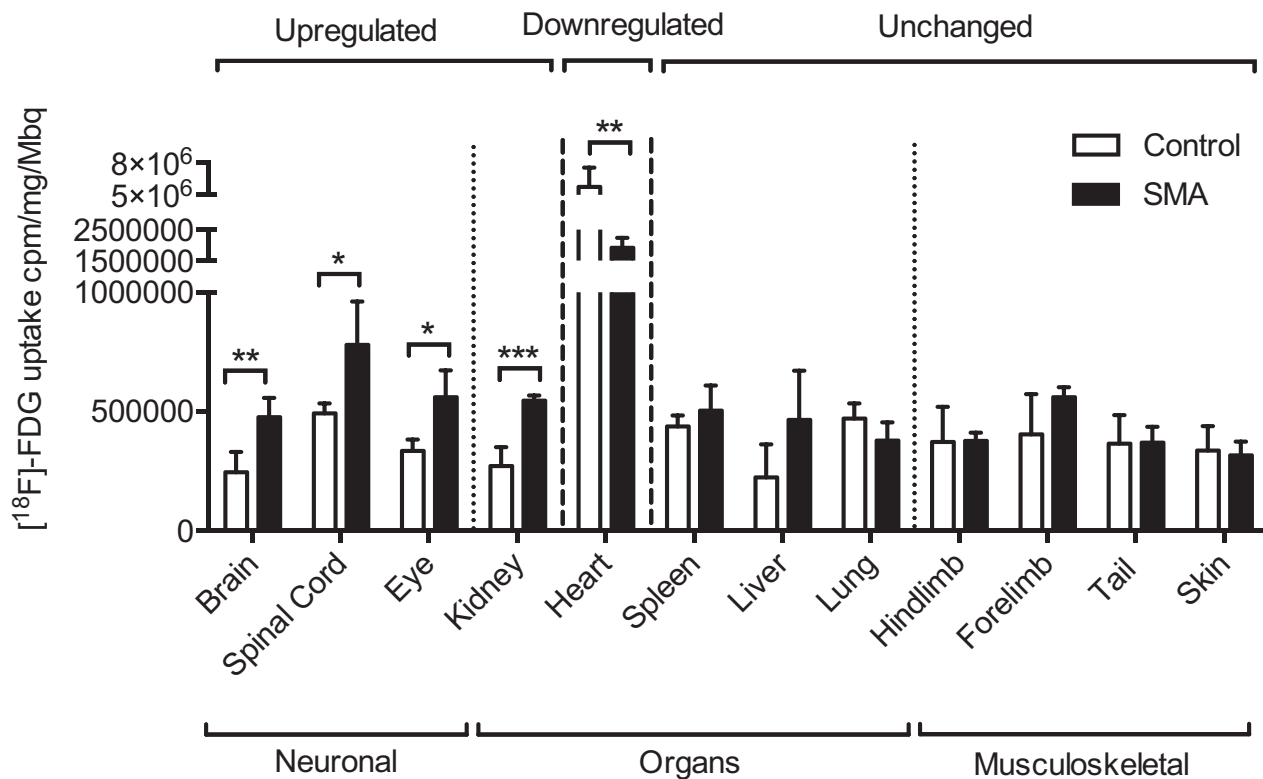


Figure 3. P5 mice show increased glucose uptake in neural tissue and kidney. Presymptomatic 5-day-old Taiwanese mice were injected with [¹⁸F]-FDG, a radioactive glucose analogue. Radioactivity was measured postmortem as counts per minute (cpm) in a well counter, and analyzed later as cpm per mg of tissue per MBq of [¹⁸F]-FDG injected (n = 4). Brain, eyes, spinal cord, and kidneys showed upregulation of [¹⁸F]-FDG uptake compared to their healthy control littermates, which is consistent with widespread hypoxia in SMA mouse model. [¹⁸F]-FDG uptake remains similar in spleen, liver, lungs, hindlimbs, forelimbs and skin. Central nervous system structures in SMA mice showed increased glucose uptake: ~58% in spinal cord (control = $4.93 \times 10^5 \pm 2.10 \times 10^4$, SMA = $7.80 \times 10^5 \pm 9.09 \times 10^4$; $P < 0.05$ *; cpm/mg mean \pm SEM), ~94% in brain (control = $2.46 \times 10^5 \pm 4.30 \times 10^4$, SMA = $4.77 \times 10^5 \pm 4.00 \times 10^4$; $P < 0.01$ **), and ~67% in eye (control = $3.36 \times 10^5 \pm 2.33 \times 10^4$, SMA = $5.60 \times 10^5 \pm 5.64 \times 10^4$; $P < 0.05$ *). The only non-neuronal tissues that changed were kidney and heart: kidney, showed a ~101% increase in SMA mice compared to controls (control = $2.73 \times 10^5 \pm 3.94 \times 10^4$, SMA = $5.47 \times 10^5 \pm 1.05 \times 10^4$; $P < 0.001$ ***) whereas heart showed a ~67% decrease in glucose uptake (control = $5.76 \times 10^5 \pm 9.01 \times 10^5$, SMA = $1.91 \times 10^5 \pm 1.64 \times 10^5$; $P < 0.01$ **) in SMA.

“normal” levels of SMN protein are present in SMN “knockdown” populations of neurons. This overlap has been previously seen in patient cells¹⁹ and may have implications for our understanding of neuronal vulnerability in SMA.

We next correlated the responses to hypoxia with SMN levels in single neurons. To do this we first validated a methodology to reliably identify dead NSC-34 neurons in culture. A flow cytometry-specific, fixable, viability stain was used followed by a cell killing protocol by ethanol exposure. Dead neurons were identified by the fluorescence signal originating from retained viability stain, and a live/ dead filter, which identified 97.2% of ethanol killed cells in a positive control experiment (data not shown). We then applied this protocol to NSC-34 neurons maintained in normoxic or hypoxic conditions, which were then fixed, labeled for SMN

protein and analyzed by with two channel flow cytometry for SMN and the viability stain. This showed that the percentage of dead neurons increased significantly after 28h of hypoxia in SMN-KD ($P < 0.001$), but not in controls. It was also significantly higher ($P < 0.01$) in hypoxic SMN-KD compared to hypoxic controls (Figure 5B). On closer observation, dead neurons seemed to have low levels of SMN protein in all cultures (Figure 5C). Comparison of the SMN levels (mode, as skewed distributions), showed that SMN levels were significantly lower in dead cells compared to live cells in all samples ($P < 0.001$ in controls and $P < 0.01$ in SMN-KD). These data show a clear correlation between SMN levels in individual neurons and their vulnerability to hypoxia. Interestingly, low levels of SMN in control neurons also renders them vulnerable to hypoxia, and potentially other insults.

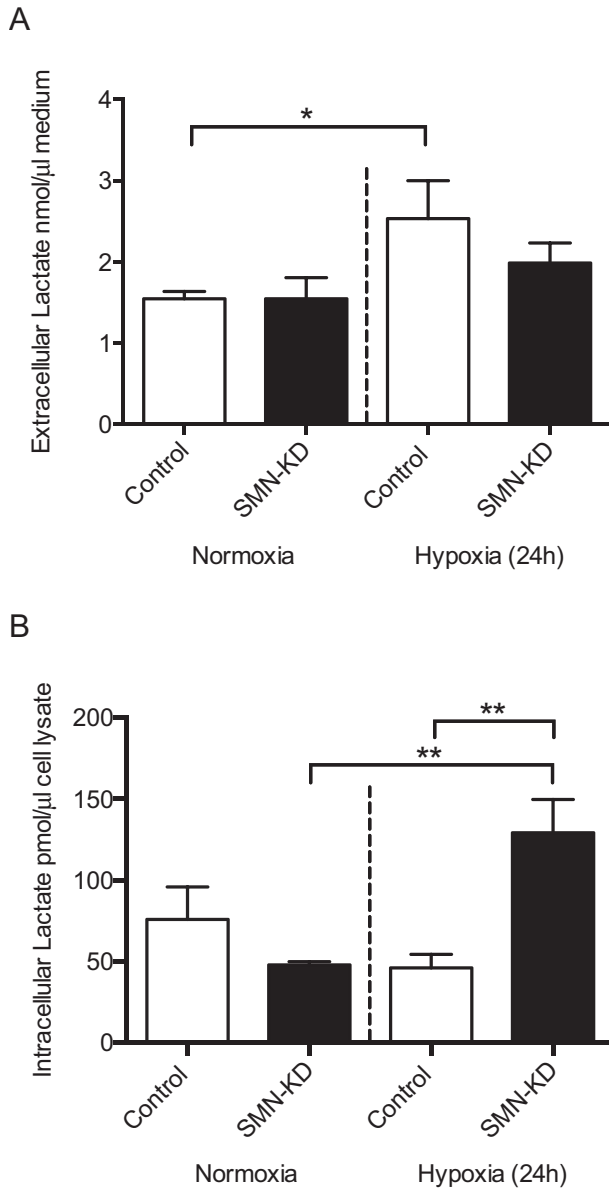


Figure 4. Intracellular L-lactate is increased after hypoxia in SMN knockdown NSC-34 neurons. A L-lactate assay detection assay kit was used to measure L-lactate production in control and SMN knockdown populations. Control and SMN knockdown populations of NSC-34 motor neurons were grown for 24 h in a hypoxic environment or in normoxic conditions. L-lactate was measured in cell culture medium and cell lysates. (A) As expected, samples of control medium had a significantly higher concentration of (extracellular) lactate in hypoxia (2.54 ± 0.27 nmol/ μ l) than in normoxia (1.55 ± 0.05 nmol/ μ l; $P < 0.05^*$). SMN knockdown neurons did not show this increase. (B) Cellular lysates from control cultures showed no change in intracellular lactate in normoxic compared to hypoxic conditions. In contrast cultures of SMN knockdown neurons in hypoxia contained 129.2 ± 11.87 pmol/ μ l of intracellular lactate compared to 47.99 ± 1.07 pmol/ μ l in normoxic SMN knockdowns ($P < 0.01^{**}$), and 46.11 ± 4.80 pmol/ μ l; $P < 0.01^{**}$) in hypoxic controls. For all conditions $n = 3$ cultures.

Cell cycle is dysregulated in SMA neurons in response to hypoxia

Altered cell cycle has previously been reported in SMA,¹⁵ and is a precursor to cell death. Therefore, in order to better understand cell death in SMA neurons in hypoxia, cell cycle was analyzed in control and SMN knockdown NSC-34 neurons in normoxia or hypoxia for 24 hours. Cell cycle was quantified by measuring DNA levels in individual neurons, using flow cytometry. The distribution of fluorescence signal and therefore of DNA content of neurons had four distinct peaks. In most proliferating mammalian cell lines the largest fluorescence peak represents neurons with a single complement of DNA in G1/G0 phase and the next highest peak represents neurons with a double complement of DNA in G2/M phase. The fluorescence peak lying between these peaks represents neurons in S phase, whereas the smallest peak with less than the single DNA complement represented dead or dying neurons (Figure 6A). Using this categorization, control and knockdown neurons showed no differences in cell cycle dynamics in normoxia (Figure 6A,B). After 24h of hypoxia, differences in cell dynamics became apparent (Figure 6A). The population of neurons in G1/G0 phase decreased significantly in controls ($P < 0.01$) and SMN-KD ($P < 0.001$), whereas the G2/M phase populations increased significantly in controls ($P < 0.01$) and SMN-KD ($P < 0.001$), although the degree of change was more pronounced in the knockdown cells. Sub-G1, dead, and dying cells increased significantly in controls ($P < 0.01$) and SMN-KD ($P < 0.05$) neurons. Numbers of neurons in S phase were consistent in all conditions. Numbers of sub-G1, dead and dying, and G2/M neurons were significantly increased, whereas G1/G0 were significantly decreased in hypoxia compared to normoxia in both control and SMN-KD neurons (Figure 6B). These represent typical responses to cell stress. However, the significant decrease in the numbers of G1/G0 and increase in the numbers of G2/M in SMN-KD neurons compared to control neurons in hypoxia suggests that mitosis is not proceeding normally in these SMA model neurons, consistent with activation of a G2/M cell cycle checkpoint.

Taken together these data demonstrate that hypoxia is a widespread stress factor in SMA, which significantly affects widespread tissues and organs, and particularly the central nervous system. This hypoxia targets cells and neurons with the lowest levels of SMN protein in both normal and SMA populations and has important downstream effects on metabolism and cell dynamics. We conclude that therapeutic investigation of methods to increase tissue oxygenation may be beneficial in SMA patients. In addition, low levels of SMN protein may be a risk factor in other neurological diseases including ALS.

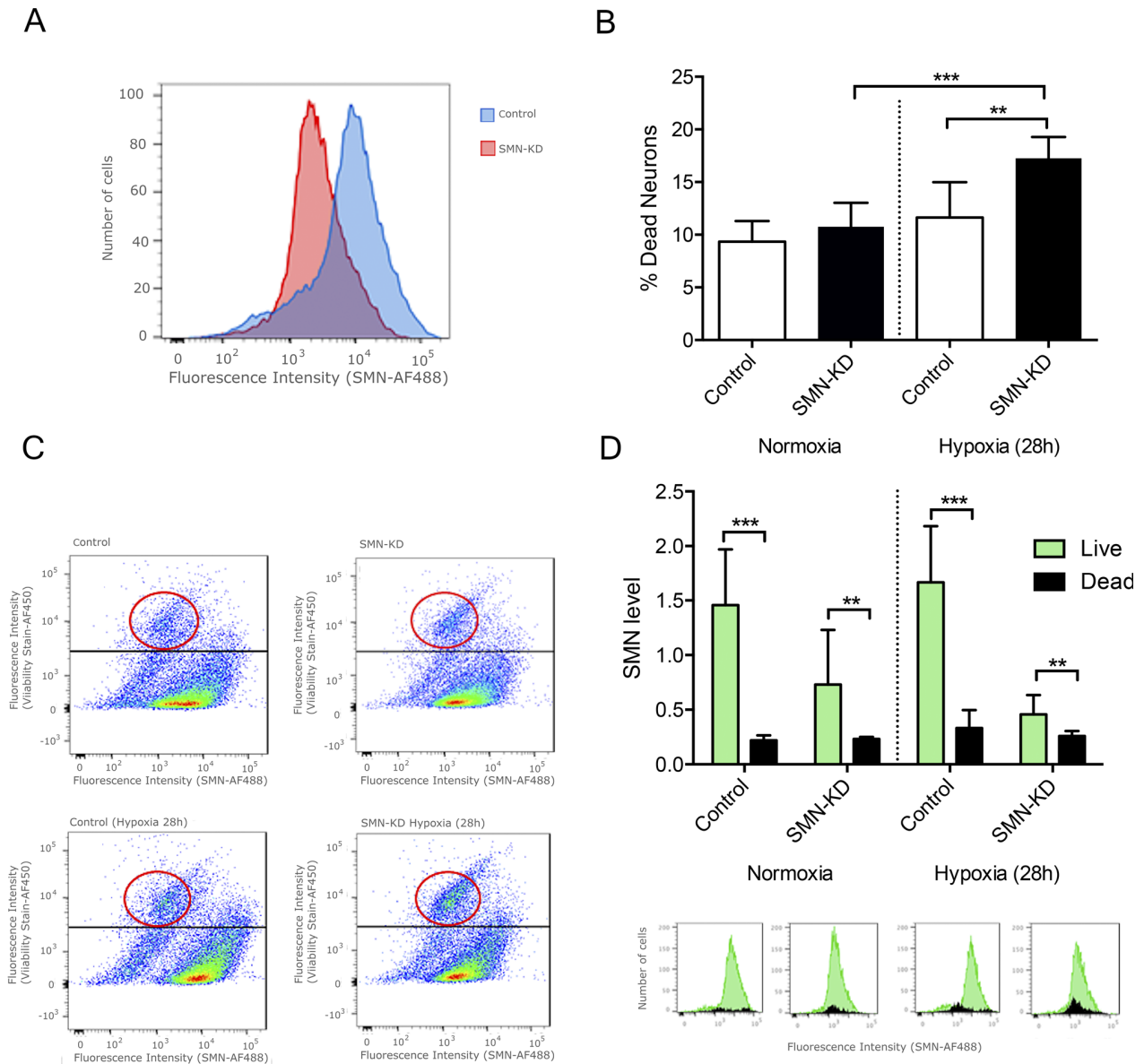


Figure 5. Low-SMN motor neurons are more sensitive to hypoxic insult. Flow cytometry was used to measure SMN levels in individual neurons in control and SMN knockdown populations. Results show great overlap between populations (A) It also shows that populations are skewed, so mode is a better representative of SMN levels than mean. Control and SMN knockdown populations of NSC-34 motor neurons were grown for 28 h in a hypoxic environment or in normoxic conditions. Flow cytometry was used to measure SMN levels and discriminate between dead and live populations. The percentage of dead neurons increased significantly after 28h of hypoxia in SMN-KD ($P < 0.001^{***}$), but not in controls. It was also significantly higher ($P < 0.01^{**}$) in SMN-KD compared to controls (B). Most dead neurons, (marked with a red circle) seem to be concentrated on the low SMN side of the spectrum in both control and knockdown samples (C). Modal SMN levels in dead and live populations were compared after being normalized to the SMN levels in the control population in normoxia, (D) and shown to be significantly different within the same sample ($P < 0.001^{***}$ in controls, $P < 0.01^{**}$ in knockdowns) after hypoxia. The SMN levels of dead cell populations in knockdown and control do not show significant difference between them. If mean SMN levels of the normoxic control neurons (dead and live) are considered as 100%, all dead cell levels were between 20-25% in normoxia and 25-35% in normoxia. In the live cell populations, control SMN levels were close to 150%, whereas SMN knockdown levels were 73% in normoxia and 46% in hypoxia.

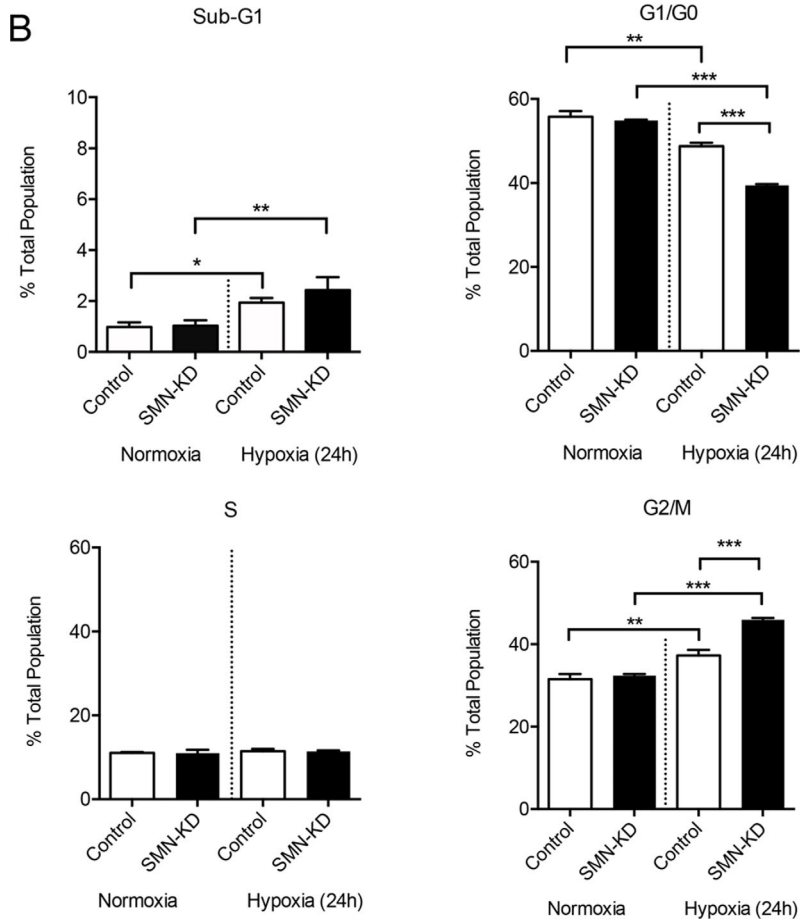
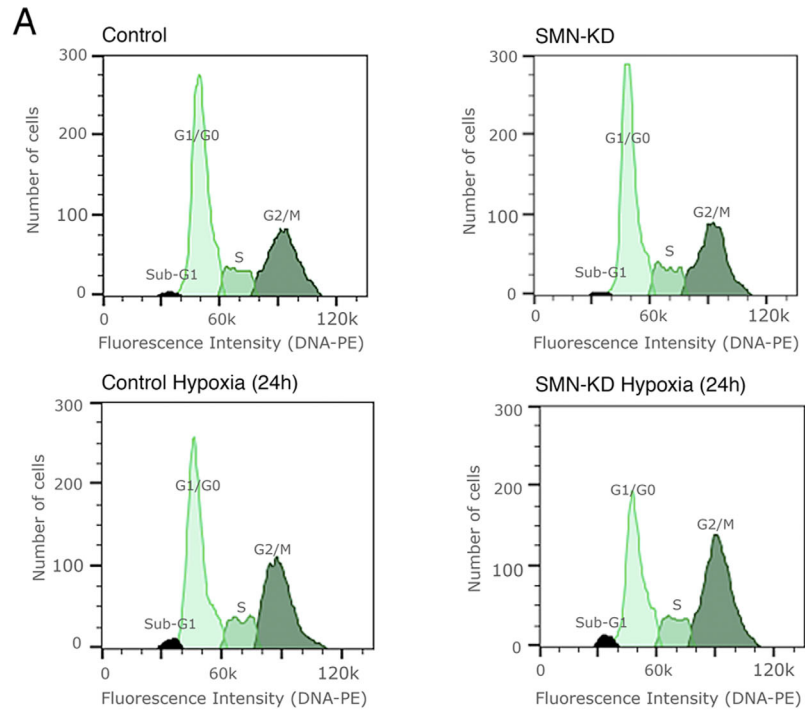


Figure 6. Cell cycle is altered in SMN-knockdown NSC-34 neurons after hypoxia. Flow cytometry was used to analyze cell cycle progression in control and SMN knockdown populations. Control and SMN knockdown populations of NSC-34 motor neurons were grown for 24 h in a hypoxic environment or in normoxic conditions. Flow cytometry was used to measure DNA levels and discriminate between sub-G1 (dead), G1/G0, S, and G2/M phase cell populations. Neurons in the lower fluorescence peak, with a single complement of DNA, were counted as G1/G0, whereas neurons in the higher peak, with double the DNA content and therefore fluorescence signal, were counted as G2/M phase neurons. Neurons with a lower than the single DNA complement of those in G1/G0 phase were counted as dead or dying, whereas neurons whose fluorescence signal was in between first and second peaks were counted as S phase (A). Control and knockdown population show the same pattern on normoxia. In both control and SMN knockdown, G1/G0 neurons in normoxia are 55% of the single cell population, and 32% are G2/M. In hypoxia, G1/G0 neurons are 49% of the population in controls and 39% in SMN knockdown neurons. G2/M cells are 37% of the population in controls and 46% in SMN knockdown neurons (B). For all conditions $n = 3$ cultures, 10,000 single cells were recorded per sample.

Discussion

The most significant, life limiting pathology in SMA is that of the neuromuscular system, and it is clear that motor neurons are selectively vulnerable to the low levels of SMN protein which characterize the disease. However, it is now also clear that a number of non-neuronal tissues also show disease-related pathology, and that the cardiovascular system is particularly involved, with heart, vessels, and circulating cells all described as pathological in severe mouse models and now also increasingly in patients. We were keen to understand the extent to which vascular dysfunction could contribute to and potentially exacerbate motor neuron death, having previously shown decreased vasculature associated with tissue hypoxia in spinal cord.

Hypoxia is widespread in neuronal and non-neuronal tissues in pre/early-symptomatic SMA mice

Here we show using qualitative (pimonidazole uptake) (Figure 1) and quantitative ([¹⁸F]-FAZA uptake and measurement) (Figure 2) techniques that a wide range of tissues from brain and eye, through skeletal muscle to visceral organs are significantly hypoxic at pre/early symptomatic time points. Importantly skin and lung, which can absorb atmospheric oxygen, showed no evidence of hypoxia. This immediately suggests a need to assess SMA patients, and particularly those undergoing therapy, for ongoing, perhaps low-level chronic hypoxia, and also potential utilization of oxygenation as an easy to deliver, ameliorative, therapy.²⁰

There is evidence of pathologies which may be associated with chronic hypoxia in SMA: thalamic lesions in type I SMA patients²¹; cerebral atrophy, EEG abnormalities, or widespread neuronal degeneration in type 0 SMA.²² Of particular interest are SMA patient MRIs resemble those taken from patients with perinatal hypoxic-ischemic brain injury.²²

Chronic hypoxia induces or exacerbates neurodegeneration in the central nervous system (CNS), where it is associated with neuroinflammation and/or mitochondrial malfunction.²³ Chronic CNS hypoxia increases

inflammation,²⁴ and the prolonged neuroinflammation in SMA,²⁵ has negative effects on cell survival.²⁶ Hypoxic neurons lose synapses, show deficits in long-term synaptic plasticity,²⁷ and can develop mitochondrial pathology, exacerbating existing pathologies in SMA.²⁸

SMA muscle shows significantly delayed myotube development and myoblast defects,²⁹ both of which also occur in hypoxia. Recent work showed a decrease in muscle oxygenation during exercise in patients with mild SMA,³⁰ indicative of an inefficient cardiovascular system which fails to compensate during exercise. Chronic hypoxia can cause muscle fibers to lose myofibrillar proteins and mitochondria, likely to both reduce size, and as a consequence the distance between capillaries, and to reduce the amount of reactive oxygen species (ROS) produced by the mitochondria.³¹

Little is known of the effects of chronic hypoxia in visceral organs, but heart defects are common in SMA patients, and mouse models show developmental alterations.^{16,32} Congenital heart defects result in myocardial hypoxia at early developmental stages, and the surgical risk factor in operated children appears to be correlated directly to the level of hypoxia in the heart, as it has a detrimental effect on myocardial metabolism and function.³³ Chronic hypoxia also results in defective ventricular function and anomalies in the enzymes involved in glycogen storage, aerobic, and anaerobic glycolysis.³³ Current SMA treatments do not target the heart, which become more vulnerable to hypoxia over time.⁹ Chronic hypoxia occurs in chronic renal disease and is associated with increased apoptosis in the renal tubules³⁴ and increased renal fibrosis, which in turn damages glomeruli and the accompanying peritubular capillaries and could exacerbate vascular pathology and hypoxia.

Glucose and lactate metabolism are dysregulated in SMA mice

A key question was what the effect of chronic hypoxia might be on cells and tissues with low levels of SMN protein. Brain, spinal cord, eye, and kidney all showed an increase in [¹⁸F]-FDG uptake, whereas heart showed a

decrease in SMA mice (Figure 3). This dysregulation of key metabolism likely has considerable downstream metabolic consequences. The decrease in heart was most surprising, but as heart rate is lower in SMA mice, this could account for the decreased glucose uptake, as lower activity means lower energy requirements.³⁵ The hypoxia response is correlated with metabolic changes, which helps to explain the response in the other tissues.³⁶

Another feature of the metabolic changes in SMA is an increase in lactate accumulation. Both intracellular and extracellular lactate showed a predicted shift to lactate synthesis in hypoxic NSC-34 neurons, but in hypoxia SMN-KD NSC-34 neurons do not properly transport the lactate out of the cell, resulting in toxic lactate accumulating in the intracellular compartment (Figure 4).

Blocking of the main lactate transporter, MCT4, results in lactate accumulation and acidification of the cytoplasm, increasing the apoptosis ratio.³⁷ While it is not clear if this defect is causing the lactate accumulation in SMA neurons, the effects may be similar. In each case, these are fundamental metabolic defects manifesting in SMN knockdown cells when exposed to the cell stress of hypoxia. Several other groups have shown similar stress-induced defects in SMA cells, including Schwann cells.³⁸

SMN protein levels in single neurons determines survival in hypoxia

We show that neurons with low levels of SMN are more sensitive to hypoxia and will be the ones which undergo cell death first in any population (Figure 5). Given that the cellular response to hypoxia can be quite complex, resulting in either a protective effect or the induction of apoptosis,³⁹ it is possible that the reduction in SMN levels alters this balance in favor of apoptosis. Caspase 3, which is upregulated in SMN knockdown cells, activates the P53 apoptosis pathway, which is the same apoptosis pathway activated by hypoxia and HIF-1.⁴⁰ Other p53 downstream genes, like Bax, are also increased in SMA mouse spinal cord and knocking it out results in improved lifespan.⁴¹ These data show a clear link between disease hallmark low SMN levels and increased liability to undergo cell death.

Cell cycle is dysregulated in SMA neurons in response to hypoxia

Alterations in cell cycle can be a sign of cell damage,⁴² and cell cycle defects have previously been reported in SMA.¹⁵ Cells were analyzed earlier (24 rather than 28 hours) to look for changes prior to significant apoptosis. Hypoxia leads to a decrease in cells in G1/G0 and an

increase in cells in G2/M phases. These changes were exacerbated in the SMN knockdown cultures, but as S phase was unchanged, it is likely that the cell cycle is being arrested before or during mitosis (Figure 6) Cell cycle arrest at mitosis can be damaging to the cells, to the point that some cancer drugs are designed with this intent.⁴³

While hypoxia and HIF-1 response can result in cell cycle arrest, this occurs at G1/G0 phase, not at G2/M,⁴⁴ suggesting that this may be correlated to cellular stress, and not the hypoxia response. Hypoxia can block or delay mitosis,⁴⁵ and cause DNA damage,⁴⁶ which can delay mitosis for several hours. Additionally, hypoxia induced ROS species and ATP depletion, affect the mitotic spindle.⁴⁷

SMN reduction has also been connected to alterations in cell cycle pathways.⁴⁸ Cyclin G1 is overexpressed and contributes to cell cycle arrest at G2/M in case of DNA damage^{48,49} and Gtse1 overexpression, also induced by DNA damage, delays G2/M transition.^{48,50} It seems likely that the DNA damage that occurs during hypoxia is most likely triggering the increase in cells in G2/M phase.

Future perspectives

The only widely approved treatment in broad usage against SMA; nusinersen/ Spinraza, is not a systemic treatment, which means the vascular system, and the associated hypoxia, are not being treated in most of the organism. These results suggest that hypoxia is a widespread pathology that is particularly damaging to SMN knockdown cells. The resultant metabolic changes which include altered essential glucose and lactate handling, stalled cell cycle, and resultant cell death deserve serious consideration. The likely exacerbating effects on existing pathologies, emphasizes the need to monitor and treat SMA as a systemic disease.

Acknowledgments

SHP, EH-G, INF, SD'A, and JMC were funded by SMA Europe (SMA UK and Prinses Beatrix Spierfonds). Thanks to Prof Andy Welch for helpful discussions on imaging.

Authors' Contributions

EH-G, INF, and SHP involved in conception, design of the study, and acquisition and analysis of data. SD'A and JMC involved in acquisition and analysis of data.

Conflict of Interest

The authors report no conflicts of interest.

References

1. Monani UR, Lorson CL, Parsons DW, et al. A single nucleotide difference that alters splicing patterns distinguishes the SMA gene SMN1 from the copy gene SMN2. *Hum Mol Genet* 1999;8:1177–1183.
2. Singh RN, Howell MD, Ottesen EW, Singh NN. Diverse role of survival motor neuron protein. *Biochim Biophys Acta - Gene Regul Mech* 2017;1860(3):299–315.
3. Monani UR, Sendtner M, Coovert DD, et al. The human centromeric survival motor neuron gene (SMN2) rescues embryonic lethality in *Smn(-/-)* mice and results in a mouse with spinal muscular atrophy. *Hum Mol Genet* 2000;9:333–339.
4. Rudnik-Schöneborn S, Vogelgesang S, Armbrust S, et al. Digital necroses and vascular thrombosis in severe spinal muscular atrophy. *Muscle Nerve* 2010;42:144–147.
5. Somers E, Lees RD, Hoban K, et al. Vascular defects and spinal cord hypoxia in spinal muscular atrophy. *Ann Neurol* 2016;79:217–230.
6. Watzlawik JO, Kahoud RJ, O'Toole RJ, et al. Abbreviated exposure to hypoxia is sufficient to induce CNS dysmyelination, modulate spinal motor neuron composition, and impair motor development in neonatal mice. *PLoS One* 2015;10:e0128007.
7. Miyazaki K, Ohta Y, Nagai M, et al. Disruption of neurovascular unit prior to motor neuron degeneration in amyotrophic lateral sclerosis. *J Neurosci Res.* 2011;89:718–728.
8. Bebee TW, Dominguez CE, Samadzadeh-Tarighat S, et al. Hypoxia is a modifier of SMN2 splicing and disease severity in a severe SMA mouse model. *Hum Mol Genet* 2012;21:4301–4313.
9. Hensel N, Kubinski S, Claus P. The need for SMN-independent treatments of spinal muscular atrophy (SMA) to complement SMN-enhancing drugs. *Front Neurol* 2020;11.
10. Javaheri S, Barbe F, Campos-Rodriguez F, et al. Sleep apnea: types, mechanisms, and clinical cardiovascular consequences. *J Am Coll Cardiol* 2017;69:841–858.
11. Sedel F, Bernard D, Mock DM, Tourbah A. Targeting demyelination and virtual hypoxia with high-dose biotin as a treatment for progressive multiple sclerosis. *Neuropharmacology* 2016;110:644–653.
12. Hsieh-Li HM, Chang JG, Jong YJ, et al. A mouse model for spinal muscular atrophy. *Nat Genet* 2000;24:66–70.
13. Smith TAD, Zanda M, Fleming IN. Hypoxia stimulates 18F-Fluorodeoxyglucose uptake in breast cancer cells via Hypoxia inducible Factor-1 and AMP-activated protein kinase. *Nucl Med Biol* 2013;40:858–864.
14. Lamidi OF, Sani M, Lazzari P, et al. The tubulysin analogue KEMTUB10 induces apoptosis in breast cancer cells via p53, Bim and Bcl-2. *J Cancer Res Clin Oncol* 2015;141:1575–1583.
15. Szunyogova E, Zhou H, Maxwell GK, et al. Survival Motor Neuron (SMN) protein is required for normal mouse liver development. *Sci Rep* 2016;6:34365.
16. Maxwell GK, Szunyogova E, Shorrock HK, et al. Developmental and degenerative cardiac defects in the Taiwanese mouse model of severe spinal muscular atrophy. *J Anat* 2018;232:965–978.
17. Fleming In, Manavaki R, Blower Pj, et al. Imaging tumour hypoxia with positron emission tomography. *Br J Cancer* 2015;112:238–250.
18. Groen EJM, Perenthaler E, Courtney NL, et al. Temporal and tissue-specific variability of SMN protein levels in mouse models of spinal muscular atrophy. *Hum Mol Genet* 2018;27:2851–2862.
19. Arakawa R, Arakawa M, Kaneko K, et al. Imaging flow cytometry analysis to identify differences of survival motor neuron protein expression in patients with spinal muscular atrophy. *Pediatr Neurol* 2016;61:70–75.
20. Desai RA, Davies AL, Tachrount M, et al. Cause and prevention of demyelination in a model multiple sclerosis lesion. *Ann Neurol* 2016;79:591–604.
21. Ito Y, Kumada S, Uchiyama A, et al. Thalamic lesions in a long-surviving child with spinal muscular atrophy type I: MRI and EEG findings. *Brain Dev* 2004;26:53–56.
22. Harding BN, Kariya S, Monani UR, et al. Spectrum of neuropathophysiology in spinal muscular atrophy type I. *J Neuropathol Exp Neurol* 2015;74:15–24.
23. Zhang F, Niu L, Li S, Le W. Pathological impacts of chronic hypoxia on Alzheimer's disease. *ACS Chem Neurosci* 2019;10:902–909.
24. Smith Stephanie M. C., Friedle Scott A., Watters Jyoti J. Chronic Intermittent Hypoxia Exerts CNS Region-Specific Effects on Rat Microglial Inflammatory and TLR4 Gene Expression. *PLoS ONE* 2013;8:e81584. <http://dx.doi.org/10.1371/journal.pone.0081584>
25. Papadimitriou D, Le Verche V, Jacquier A, et al. Inflammation in ALS and SMA: Sorting out the good from the evil. *Neurobiology of Disease* 2010;37:493–502.
26. Calsolaro V, Edison P. Neuroinflammation in Alzheimer's disease: Current evidence and future directions. *Alzheimer's and Dementia* 2016;12:719–732.
27. Almado CEL, Machado BH, Leão RM. Chronic intermittent hypoxia depresses afferent neurotransmission in NTS neurons by a reduction in the number of active synapses. *J Neurosci* 2012;32:16736–16746.
28. Acsadi G, Lee I, Li X, et al. Mitochondrial dysfunction in a neural cell model of spinal muscular atrophy. *J Neurosci Res* 2009;87:2748–2756.
29. Martínez-Hernández R, Soler-Botija C, Also E, et al. The developmental pattern of myotubes in spinal muscular atrophy indicates prenatal delay of muscle maturation. *J Neuropathol Exp Neurol* 2009;68:474–481.
30. Montes J, Goodwin, A:McDermott, M, et al. Diminished muscle oxygenation during exercise in ambulatory spinal

- muscular atrophy patients (P4.4-024). *Neurology* 2019;92: P4.4-024.
31. Murray AJ. Metabolic adaptation of skeletal muscle to high altitude hypoxia: How new technologies could resolve the controversies. *Genome Med* 2009;1:117.
 32. Rudnik-Schöneborn S, Heller R, Berg C, et al. Congenital heart disease is a feature of severe infantile spinal muscular atrophy. *J Med Genet* 2008;45:635–638.
 33. Najm HK, Wallen WJ, Belanger MP, et al. Does the degree of cyanosis affect myocardial adenosine triphosphate levels and function in children undergoing surgical procedures for congenital heart disease? *J Thorac Cardiovasc Surg* 2000;119:515–524.
 34. Khan S, Cleveland RP, Koch CJ, Schelling JR. Hypoxia induces renal tubular epithelial cell apoptosis in chronic renal disease. *Lab Invest* 1999;79:1089–1099.
 35. Heier CR, Satta R, Lutz C, Didonato CJ. Arrhythmia and cardiac defects are a feature of spinal muscular atrophy model mice. *Hum Mol Genet* 2010;19:3906–3918.
 36. Wood IS, Wang B, Lorente-Cebrián S, Trayhurn P. Hypoxia increases expression of selective facilitative glucose transporters (GLUT) and 2-deoxy-d-glucose uptake in human adipocytes. *Biochem Biophys Res Commun* 2007;361:468–473.
 37. Zhao Y, Li W, Li M, et al. Targeted inhibition of MCT4 disrupts intracellular pH homeostasis and confers self-regulated apoptosis on hepatocellular carcinoma. *Exp Cell Res* 2019;384(1):111591.
 38. Hunter G, Powis RA, Jones RA, et al. Restoration of SMN in Schwann cells reverses myelination defects and improves neuromuscular function in spinal muscular atrophy. *Hum Mol Genet* 2016;25:2853–2861.
 39. Piret JP, Mottet D, Raes M, Michiels C. Is HIF-1 α a pro- or an anti-apoptotic protein? *Biochem Pharmacol* 2002;64:889–892.
 40. Parker GC, Li X, Anguelov RA, et al. Survival motor neuron protein regulates apoptosis in an in vitro model of spinal muscular atrophy. *Neurotox Res* 2008;13:39–48.
 41. Tsai MS, Chiu YT, Wang SH, et al. Abolishing bax-dependent apoptosis shows beneficial effects on spinal muscular atrophy model mice. *Mol Ther* 2006;13:1149–1155.
 42. Barnum KJ, O'Connell MJ. Cell cycle regulation by checkpoints. *Methods Mol Biol* 2014;1170:29–40.
 43. Weaver BAA, Cleveland DW. Decoding the links between mitosis, cancer, and chemotherapy: The mitotic checkpoint, adaptation, and cell death. *Cancer Cell* 2005;8:7–12.
 44. Iida T, Mine S, Fujimoto H, et al. Hypoxia-inducible factor-1 α induces cell cycle arrest of endothelial cells. *Genes Cells* 2002;7:143–149.
 45. Fischer MG, Heeger S, Häcker U, Lehner CF. The mitotic arrest in response to hypoxia and of polar bodies during early embryogenesis requires *Drosophila* Mps1. *Curr Biol* 2004;14:2019–2024.
 46. Barzilai A, Yamamoto KI. DNA damage responses to oxidative stress. *DNA Repair* 2004;3:1109–1115.
 47. Burgess A, Rasouli M, Rogers S. Stressing mitosis to death. *Front Oncol* 2014;4.
 48. Staropoli JF, Li H, Chun SJ, et al. Rescue of gene-expression changes in an induced mouse model of spinal muscular atrophy by an antisense oligonucleotide that promotes inclusion of SMN2 exon 7. *Genomics* 2015;105:220–228.
 49. Kimura SH, Ikawa M, Ito A, et al. Cyclin G1 is involved in G2/M arrest in response to DNA damage and in growth control after damage recovery. *Oncogene* 2001;20:3290–3300.
 50. Monte M, Benetti R, Buscemi G, et al. The cell cycle-regulated protein human GTSE-1 controls DNA damage-induced apoptosis by affecting p53 function. *J Biol Chem* 2003;278:30356–30364.